

Generative diffusion model for surface structure discovery

Nikolaj Rønne,¹ Alán Aspuru-Guzik,^{2,3,4,5,6} and Bjørk Hammer¹

¹*Center for Interstellar Catalysis, Department of Physics and Astronomy, Aarhus University, DK-8000 Aarhus, Denmark*

²*Department of Chemistry, University of Toronto, Toronto, Ontario, M5S 3H6, Canada.*

³*Department of Computer Science, University of Toronto, Toronto, Ontario, M5S 2E4, Canada.*

⁴*Vector Institute for Artificial Intelligence, Toronto, Ontario, M5G 1M1, Canada.*

⁵*Acceleration Consortium, Toronto, Ontario, M5S 3H6, Canada*

⁶*Canadian Institute for Advanced Research, Toronto, Ontario, M5G 1M1, Canada*

(Dated: July 3, 2024)

We present a generative diffusion model specifically tailored to the discovery of surface structures. The generative model takes into account substrate registry and periodicity by including masked atoms and z -directional confinement. Using a rotational equivariant neural network architecture, we design a method that trains a denoiser-network for diffusion alongside a force-field for guided sampling of low-energy surface phases. An effective data-augmentation scheme for training the denoiser-network is proposed to scale generation far beyond structure sizes represented in the training data. We showcase the generative model by investigating multiple surface systems and propose an atomistic structure model for a previously unknown silver-oxide domain-boundary of unprecedented size.

The discovery of new stable and functional materials is a prerequisite in future technological advancements in fields such as catalysis, drug discovery, carbon-capture and energy storage.[1] The design-space of stable atomistic structures is governed by quantum mechanics and it is both vast and highly complex. Generative diffusion models have proven highly capable of tackling the similarly vast design-space of images and are therefore proposed to be a natural extension to ab-initio methods for materials discovery.

The use of generative modeling in materials science has seen rapid development in recent years by utilizing variational autoencoders[2–7], generative adversarial networks[8–11], autoregressive models[12–14], reinforcement learning[15–20], language models[21–23], normalizing flows[24–27] and diffusion models[28–39]. Most developments have been in the regime of *molecular* materials with fewer generative methods tackling the more complicated case of *periodic* materials. Diffusion models lend themselves especially well to atomistic modelling due to the few architectural requirements as compared to other methods.[40] Previous work on generative diffusion modeling of periodic materials has focused either on foundation models for discovery of bulk structures[28, 31, 33, 35] or discovery of mono-layer materials with no support[30, 36]. The seminal work by Xie et al.[28], tackling bulk structure generation, uses a diffusion model as the decoder in a variational autoencoder to address the inversion problem in materials discovery. A prerequisite for these developments in generative modeling of periodic materials is the advent of equivariant machine learning force-fields (MLFF)[41–44]. These network architectures are able to fully capture the symmetries of periodic materials in 3D and open the possibility to design equivariant score-based diffusion models by utilizing the vectorial atom embeddings to predict vectorial

scores.

In this work, we leverage the new developments in generative modelling and naturally extend it to surface structure discovery. We introduce a generative diffusion method specifically tailored to surface supported thin-films by including masked substrate atoms and a z -directional confinement. Furthermore, we introduce a force-field-guidance framework for sampling by introducing learned atomic forces into the sampling process and an efficient data-augmentation technique to extent model stability to larger systems. We show the superiority of the diffusion based generation method by comparison to random structure search[45] (RSS) for multiple surface systems. Furthermore, we solve a domain-boundary problem for a silver-oxide on Ag(111).

Generative diffusion models rely on learning to denoise deliberately corrupted data hereby establishing a denoiser-network. The trained denoiser-network can then be used to sample from the underlying data distribution. Both the forward data-corruption process and the reversed generation process can be formulated as stochastic differential equations (SDE). The denoiser-network naturally appears in the reversed SDE as the score function, s , defined as the derivative of the log-transformed data probability distribution.[46]

A periodic atomistic structure is fully described by $\mathcal{M} = (\mathbf{z}, \mathbf{R}, \mathbf{S})$ representing the atomic types, atomic positions and periodic cell. In this work, we keep atomic types and cell fixed through the diffusion process. We define a forward diffusion process acting on the atomic positions through a SDE as

$$d\mathcal{M} = -\frac{1}{2}\beta(t)\mathcal{M}dt + \sqrt{\beta(t)}d\mathcal{W}, \quad (1)$$

where $t \in [0, 1]$ is time, $\beta(t) = \beta_{\min} + t(\beta_{\max} - \beta_{\min})$ is a linearly increasing function between β_{\min} and β_{\max} ,

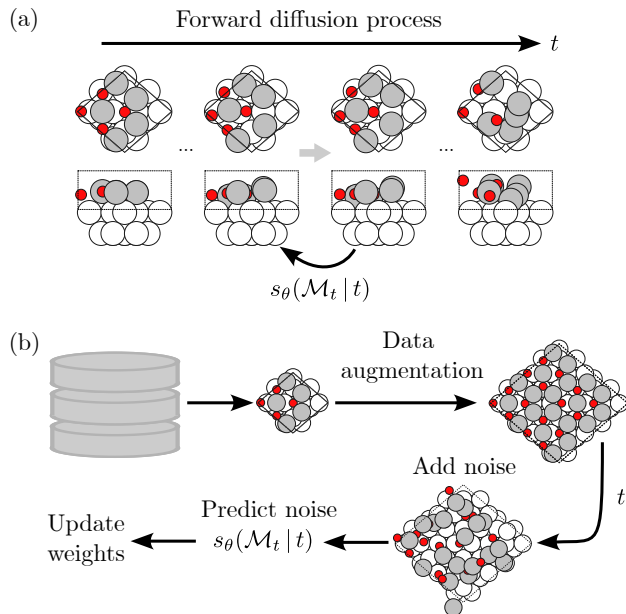


FIG. 1. (a) Schematic of the forward diffusion process where a small amount of noise is added at each step. At the final step the atomic positions correspond to being drawn from a uniform distribution. The denoiser-network, $s_{\theta}(\mathcal{M}_t | t)$, learns to predict the added noise at any given time-step t . (b) The process for training the denoiser-network. A training step is comprised of drawing a sample, performing data-augmentation through periodic repetition of sample, drawing a random time $t \in [0, 1]$, corrupt the sample corresponding to t , predict the added noise using the denoiser-network and finally use the disagreement between added and predicted noise to update the denoiser-network weights.

and $d\mathcal{W}$ is infinitesimal Brownian noise.[46] The coefficients of the terms are typically referred to as *drift* and *diffusion* coefficient respectively. The forward diffusion process is analytical and can be discretized and sampled. We index the discretized diffusion process by the time variable, which together with a known noise distribution allows a direct forward sampling of noisy structures. Intuitively the forward SDE represents the iterative addition of Gaussian noise to the atomic positions as illustrated in Fig. 1(a). The reversed diffusion process can also be formulated as a SDE and is given as

$$d\mathcal{M} = \left[-\frac{1}{2}\beta(t)\mathcal{M} - \beta(t)s(\mathcal{M}) \right] dt + \sqrt{\beta(t)}d\tilde{\mathcal{W}}, \quad (2)$$

where $s(\mathcal{M})$ is the unknown score function and $d\tilde{\mathcal{W}}$ is reverse-time Brownian noise. We design a network that approximates the score function, $s_{\theta}(\mathcal{M} | t)$, given a structure and a time conditioning $t \in [0, 1]$ and will refer to this as the denoiser-network. The denoiser-network, $s_{\theta}(\mathcal{M} | t)$, is trained by predicting the vectorial noise added at any given time, t , through denoising score-matching[40] as illustrated in Fig. 1(b). The architec-

ture of the denoiser-network is a time-conditioned non-conservative vector-field regressor implemented using the equivariant PaiNN [42] architecture cf. SI Fig. 1 for more details.

The denoiser-network training process is outlined schematically in Fig. 1(b) and is presented in detail in the following. First, a database of stable atomistic structures is procured. In this work we, either perform RSS for multiple stoichiometries in small periodic cells and gather the lowest energy structures, or we use a previously established dataset. The specific composition of the dataset is highly influential on the later generated structures as it defines the data probability distribution that is sampled from. This acts as a data bias, that can be used to drive generation towards specific areas of configurational space. Specifically we select low-energy structures as training data. A further discussion of this is provided in the supplementary material. For all cases, we use smaller systems for training data than the system we use for testing, since these are feasible to evaluate with DFT. Furthermore this ensures that we showcase out-of-distribution generalizability of the generative model. Second, we perform data-augmentation by repeating the training data periodically, such that the effective number of atoms in the training data materials increases. This allows the denoiser-network to learn interactions between a higher number of atoms at no cost of procuring additional training data for larger cell-sizes. This data-augmentation technique can equally well be used for bulk materials and ensures stability of the denoiser-network when many atoms are close. The extent of data-augmentation needed depends on the expected size of the test systems. Third, denoising score-matching is used to train the denoiser network. Here, a random timestep, $t \in [0, 1]$, is sampled and the training example is noised according to the forward diffusion process. The denoiser-network is then used to predict the noise added to the training example based on the noisy structure and conditioned on t . The network loss is the discrepancy between the actual noise and the predicted noise, taking periodic boundary conditions into account, which is then used to update the network weights.[28] In practice training is performed with batches of data.

We introduce two specific developments tailoring the diffusion model to surface structure generation. First, we use truncated Gaussian distribution in the z -direction perpendicular to the substrate surface, while we use a standard Gaussian distribution in the periodic directions cf. SI Fig. 2. Hereby, we ensure that generated structures only form surface structures on one side of the finite substrate. Second, substrate atoms are masked in the diffusion process, hereby fixing the atoms. Masking substrate atoms is key when studying surface systems as the substrate is often experimentally known, whereas the overlayer is what dictates the physical and chemical properties.[47] In previous work[30], substrate inter-

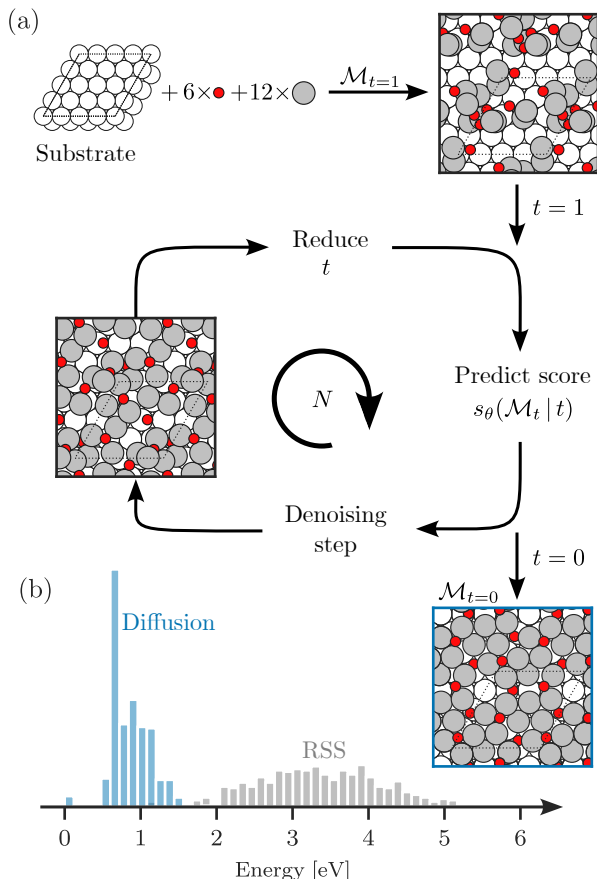


FIG. 2. (a) Sampling process exemplified with the $p(4 \times 4)$ AgO surface structure. The $t = 1$ structure is initialized at random. N denoising steps are performed following Eq. 2 using the predicted score from the denoiser-network and slowly annealing t . The $p(4 \times 4)$ structure sampled from the diffusion process is presented. (b) Comparison between diffusion-based sampling and RSS for Ag_{12}O_6 in the $p(4 \times 4)$ cell.

actions have been neglected, while we introduce a masked substrate that allows for the direct discovery of surface and registry dependent structural models.

Sampling from a diffusion model consists of following the reversed diffusion process described by Eq. 2 using the trained denoiser-network and is schematically presented in Fig. 2(a). First, the test substrate and the pre-specified number of atoms is initialized according to the known prior noise distribution, which is a uniform distribution of each atom within the periodic cell. The prior noise distribution is intuitively understood as the distribution obtained by iterative application of Gaussian noise. We use the Ag(111)- $p(4 \times 4)$ cell with stoichiometry Ag_{12}O_6 representing the cell and stoichiometry of the known “Ag₆ model” as an example in Fig. 2(a). Second, the time-variable, $t \in \{1, \dots, 0\}$, is discretized in N steps of step-length Δt . Third, N steps of a time-annealing process is performed where the denoising follows Eq. 2

using the predicted score as shown in Fig. 2(a). During sampling, the same noise distributions are used as in the forward process. Specifically in the z -direction, the truncated Gaussian distribution is used such that the atoms never leave the non-periodic confinement. We introduce force-field-guidance inspired by classifier-guidance for image generation[48], where the force-prediction of a concurrently trained MLFF, $f(\mathcal{M})$, is gradually introduced during the sampling process in order to guide the reversed diffusion towards more stable materials. The MLFF can be efficiently included in the denoiser architecture almost without additional prediction cost cf. SI Fig. 1. The force injection is controlled by the scalar function $\tau(t)$ as

$$d\hat{\epsilon} = \tau(t)f(\mathcal{M})dt, \quad (3)$$

where $\tau(t) = \eta(1 - t)$ with η a constant and $f(\mathcal{M}) = -\nabla_{\mathbf{R}}E(\mathcal{M})$. This means that, as time is decreasing during sampling, more emphasis is put onto decreasing the predicted force. $d\hat{\epsilon}$ represents an additional term in the reversed diffusion process defined by Eq. 2 and thus becomes an integrated part of the denoising step.

To judge the quality of sampled structures, we perform a comparison between diffusion-based sampling and the unbiased sampling obtained using RSS. We relax every sampled structure to provide a fair comparison in terms of energy of the generated structures. Fig. 2(b) shows a typical comparison to RSS in terms of stability of generated structures for the “Ag₆ model” system in the $p(4 \times 4)$ cell. In this case, the diffusion model is trained on small $c(4 \times 8)$ unit cell structures of varying stoichiometry generated using RSS. An example of a training structure is shown in Fig. 1(a). A detailed discussion on the choice and influence of training data is provided in the supplementary material.

Figure 2(b) evidences that the structures produced by sampling from the diffusion model are lower in energy compared to what is produced by RSS. This demonstrates that the diffusion model is capable of generalizing to larger and more complex atomistic systems. The data bias of the method is likewise transferable giving rise to a shifted and more narrow energy-distribution of samples compared to RSS. The three atomistic structural models shown as insets in Fig. 2 represents the first, middle and final structural models during a sampling trajectory. In the middle of sampling, corresponding to step $t = 0.5$, the material is clearly more ordered with local motifs starting to resemble chemically stable bonding patterns. The final material represents the “Ag₆ model” of silver-oxide on Ag(111) with a central ring, that exposes a substrate atom. We observe that the surface registry is found directly by including the masked substrate atoms in the diffusion process.

In Fig. 3 we further demonstrate that the method is generally applicable to surface structure discovery. We concurrently compare the quality and computational efficiency of diffusion and RSS. This is done by limiting the

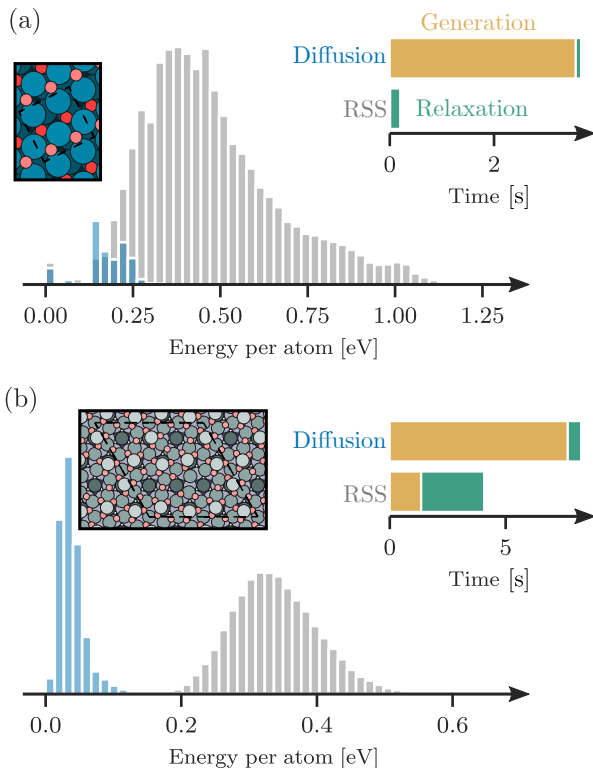


FIG. 3. Comparison between diffusion sampling and RSS with equal GPU-time for (a) Pd_4O_4 on $\text{Pd}(100)$ in a $p(\sqrt{5} \times \sqrt{5})$ cell giving rise to the $(\sqrt{5} \times \sqrt{5})\text{R}27^\circ$ surface oxide as shown in the inset. (b) $\text{Sn}_{43}\text{O}_{46}$ on $\text{Pt}_3\text{Sn}(111)$ substrate in a $p(8 \times 8)$ supercell giving rise to a defected oxide structure as presented in the inset. Furthermore, a timing comparison between diffusion and RSS detailing time spent on generation and relaxation per generated structure.

total GPU-time and generate as many candidates as possible either using RSS or diffusion. As a target potential, we use a pre-trained MLFF trained using the SchNetPack software[49, 50]. We present timings for generation and relaxation. In Fig. 3(a) we study a rather small system of PdO on $\text{Pd}(100)$ in a $p(\sqrt{5} \times \sqrt{5})$ cell giving rise to the $(\sqrt{5} \times \sqrt{5})\text{R}27^\circ$ surface oxide as shown in the inset.[51] Similar to the AgO system shown previously, the structures generated by the diffusion model are much more stable than those produced by RSS. But within the fixed GPU time-budget we are able to produce many more samples using RSS thereby giving similar performance in sampling the most stable structures. Comparing the time for generation and sampling, we see that little relaxation is needed for diffusion-generated samples, which reflects that the diffusion-produced samples are already very close to local energy minima. In Fig. 3(b) we move to a much more complicated system consisting of a defected SnO on $\text{Pt}_3\text{Sn}(111)$ substrate in a $p(8 \times 8)$ supercell. We choose the stoichiometry of $\text{Sn}_{43}\text{O}_{46}$ which deviates slightly from the known $\text{Sn}_{11}\text{O}_{12}$ stoichiometry of

the $p(4 \times 4)$ surface phase.[52] For such a complicated system it is a rare-event that RSS generates a stable structure, whereas the diffusion model is able to scale efficiently to larger systems and continue to generate highly stable samples. Furthermore, the generation time relative to RSS is not as limiting, since both generation and especially relaxation is very time-consuming with RSS. Similar to Fig. 3(a), we also see that the relaxation-time for diffusion is significantly less than for RSS again showing that the structures sampled from the diffusion model are close to local energy minima. The structural model presented in Fig. 3(b) is the most stable generated structure and represents the $p(4 \times 4)$ phase with a single SnO_2 -unit removed highly resembling the defected experimental STM images presented in Ref. [53].

To further test the out-of-domain generalizability of diffusion sampling, we use a diffusion model trained on stable silver oxides structures in the small $c(4 \times 8)$ unit cell to perform a diffusion-based structure search for a defected surface phase that has been experimentally observed in Ref. [54]. The cell size of the test system is $\sqrt{57}\text{R}6.6^\circ \times \sqrt{28}\text{R}40.9^\circ$. The screening workflow is outlined in the following. First, we generate structures with the diffusion models for varying stoichiometries as indicated in Fig. 4. Second, we perform post-relaxation of all generated structures using the universal potential CHGNet[55]. Last, we select the ten most stable structures for relaxation with DFT and evaluate the thermodynamic stability[56]. Fig. 4 presents the thermodynamic stability of the best surface phases under experimental conditions in (a) and the proposed atomistic model of the surface defect together with experimental STM hereof in (b). The proposed structural model features a very similar motif as the $c(4 \times 8)$ phase and it should be noted that all surface atoms are generated using diffusion without forcing the boundary to be that of the $c(4 \times 8)$ phase. This exemplifies the power of data-driven generation through diffusion sampling and provides a major improvement over unbiased approaches such as RSS, where discovering the stable surface defect would be unfeasible.

In conclusion, we have introduced a generative diffusion model for surface structure discovery that is shown to outperform traditional atomistic generation methods on a number of surface systems. We have shown that a data-biased generative method, even though more computationally demanding, provides more quantum mechanically relevant samples than a relaxation based approach. Finally, we have proposed a structural model to a large silver-oxide domain-boundary based on a diffusion-based structure search.

The code is publicly available under the GPLv3 license at <https://github.com/nronne/dss> and all data is available at <https://github.com/nronne/surface-diffusion-model-data>.

We acknowledge support by VILLUM FONDEN

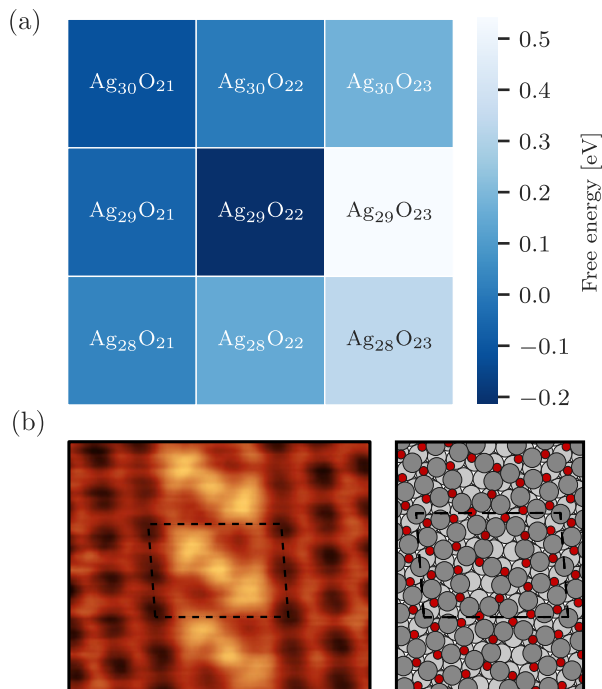


FIG. 4. (a) Thermodynamic stability of best domain-boundary structures for varying stoichiometries under experimental conditions. (b) Experimental STM and proposed structural model of the $\text{Ag}_{29}\text{O}_{22}$ domain-boundary. Experimental STM adapted with permission from ACS Catal. 2016, 6, 7, 4640–4646. Copyright 2016 American Chemical Society.

through Investigator grant, project no. 16562, and by the Danish National Research Foundation through the Center of Excellence “InterCat” (Grant agreement no: D NRF150). This research was undertaken thanks in part to funding provided to the University of Toronto’s Acceleration Consortium from the Canada First Research Excellence Fund CFREF-2022-00042. AAG thanks Anders G. Frøseth for his generous support. AAG also acknowledges the generous support of Natural Resources Canada and the Canada 150 Research Chairs program.

REFERENCES

- [1] Z. Yao, Y. Lum, A. Johnston, L. M. Mejia-Mendoza, X. Zhou, Y. Wen, A. Aspuru-Guzik, E. H. Sargent, and Z. W. Seh, *Nat Rev Mater* **8**, 202 (2023).
- [2] R. Gómez-Bombarelli, J. N. Wei, D. Duvenaud, J. M. Hernández-Lobato, B. Sánchez-Lengeling, D. Sheberla, J. Aguilera-Iparraguirre, T. D. Hirzel, R. P. Adams, and A. Aspuru-Guzik, *ACS Cent. Sci.* **4**, 268 (2018).
- [3] J. Lim, S. Ryu, J. W. Kim, and W. Y. Kim, *Journal of Cheminformatics* **10**, 31 (2018).
- [4] Q. Liu, M. Allamanis, M. Brockschmidt, and A. Gaunt, in *Advances in Neural Information Processing Systems*, Vol. 31 (Curran Associates, Inc., 2018).
- [5] W. Jin, R. Barzilay, and T. Jaakkola, in *Proceedings of the 35th International Conference on Machine Learning* (PMLR, 2018) pp. 2323–2332.
- [6] J. Noh, J. Kim, H. S. Stein, B. Sanchez-Lengeling, J. M. Gregoire, A. Aspuru-Guzik, and Y. Jung, *Matter* **1**, 1370 (2019).
- [7] Z. Yao, B. Sánchez-Lengeling, N. S. Bobbitt, B. J. Bucior, S. G. H. Kumar, S. P. Collins, T. Burns, T. K. Woo, O. K. Farha, R. Q. Snurr, and A. Aspuru-Guzik, *Nat Mach Intell* **3**, 76 (2021).
- [8] B. Kim, S. Lee, and J. Kim, *Science Advances* **6**, eaax9324 (2020).
- [9] T. Long, N. M. Fortunato, I. Opahle, Y. Zhang, I. Samathrakris, C. Shen, O. Gutfleisch, and H. Zhang, *npj Comput Mater* **7**, 1 (2021).
- [10] Y. Zhao, M. Al-Fahdi, M. Hu, E. M. D. Siriwardane, Y. Song, A. Nasiri, and J. Hu, *Advanced Science* **8**, 2100566 (2021).
- [11] M. Alverson, S. G. Baird, R. Murdock, E. Sin-Hang Ho, J. Johnson, and T. D. Sparks, *Digital Discovery* **3**, 62 (2024).
- [12] N. Gebauer, M. Gastegger, and K. Schütt, in *Advances in Neural Information Processing Systems*, Vol. 32 (Curran Associates, Inc., 2019).
- [13] C. Shi, M. Xu, Z. Zhu, W. Zhang, M. Zhang, and J. Tang, “GraphAF: A Flow-based Autoregressive Model for Molecular Graph Generation,” (2020), arxiv:2001.09382 [cs, stat].
- [14] J. Westermayr, J. Gilkes, R. Barrett, and R. J. Maurer, *Nat Comput Sci* **3**, 139 (2023).
- [15] M. S. Jørgensen, H. L. Mortensen, S. A. Meldgaard, E. L. Kolsbjerg, T. L. Jacobsen, K. H. Sørensen, and B. Hammer, *The Journal of Chemical Physics* **151** (2019).
- [16] G. Simm, R. Pinsler, and J. M. Hernandez-Lobato, in *Proceedings of the 37th International Conference on Machine Learning* (PMLR, 2020) pp. 8959–8969.
- [17] S. A. Meldgaard, J. Köhler, H. L. Mortensen, M.-P. V. Christiansen, F. Noé, and B. Hammer, *Mach. Learn.: Sci. Technol.* **3**, 015008 (2021).
- [18] J. Yoon, Z. Cao, R. K. Raju, Y. Wang, R. Burnley, A. J. Gellman, A. B. Farimani, and Z. W. Ulissi, *Mach. Learn.: Sci. Technol.* **2**, 045018 (2021).
- [19] L. A. Thiede, M. Krenn, A. Nigam, and A. Aspuru-Guzik, *Mach. Learn.: Sci. Technol.* **3**, 035008 (2022).
- [20] R. Barrett and J. Westermayr, *J. Phys. Chem. Lett.* **15**, 349 (2024).
- [21] D. Flam-Shepherd, K. Zhu, and A. Aspuru-Guzik, *Nat Commun* **13**, 3293 (2022).
- [22] N. Fu, L. Wei, Y. Song, Q. Li, R. Xin, S. S. Omeo, R. Dong, E. M. D. Siriwardane, and J. Hu, *Mach. Learn.: Sci. Technol.* **4**, 015001 (2023).
- [23] L. M. Antunes, K. T. Butler, and R. Grau-Crespo, “Crystal Structure Generation with Autoregressive Large Language Modeling,” (2024), arxiv:2307.04340 [cond-mat].
- [24] C. Zang and F. Wang, in *Proceedings of the 26th ACM SIGKDD International Conference on Knowledge Discovery & Data Mining, KDD ’20* (Association for Computing Machinery, New York, NY, USA, 2020) pp. 617–626.
- [25] M. Kuznetsov and D. Polykovskiy, *Proceedings of the*

- AAAI Conference on Artificial Intelligence **35**, 8226 (2021).
- [26] C. Ma and X. Zhang, in *Proceedings of the 30th ACM International Conference on Information & Knowledge Management*, CIKM '21 (Association for Computing Machinery, New York, NY, USA, 2021) pp. 1181–1190.
- [27] J. Köhler, M. Invernizzi, P. de Haan, and F. Noé, “Rigid Body Flows for Sampling Molecular Crystal Structures,” (2023), arxiv:2301.11355 [physics, stat].
- [28] T. Xie, X. Fu, O.-E. Ganea, R. Barzilay, and T. Jaakkola, “Crystal Diffusion Variational Autoencoder for Periodic Material Generation,” (2022), arxiv:2110.06197 [cond-mat, physics:physics].
- [29] E. Hooeboom, V. G. Satorras, C. Vignac, and M. Welling, “Equivariant Diffusion for Molecule Generation in 3D,” (2022), arxiv:2203.17003 [cs, q-bio, stat].
- [30] P. Lyngby and K. S. Thygesen, *npj Comput Mater* **8**, 1 (2022).
- [31] V. Fung, S. Jia, J. Zhang, S. Bi, J. Yin, and P. Ganesh, *Mach. Learn.: Sci. Technol.* **3**, 045018 (2022).
- [32] B. Jing, G. Corso, J. Chang, R. Barzilay, and T. Jaakkola, “Torsional Diffusion for Molecular Conformer Generation,” (2023), arxiv:2206.01729 [physics, q-bio].
- [33] Y. Zhao, E. M. D. Siriwardane, Z. Wu, N. Fu, M. Al-Fahdi, M. Hu, and J. Hu, *npj Comput Mater* **9**, 1 (2023).
- [34] T. Weiss, E. Mayo Yanes, S. Chakraborty, L. Cosmo, A. M. Bronstein, and R. Gershoni-Poranne, *Nat Comput Sci*, 1 (2023).
- [35] C. Zeni, R. Pinsler, D. Zügner, A. Fowler, M. Horton, X. Fu, S. Shysheya, J. Crabbé, L. Sun, J. Smith, R. Tomioka, and T. Xie, “MatterGen: A generative model for inorganic materials design,” (2023), arxiv:2312.03687 [cond-mat].
- [36] H. Moustafa, P. M. Lyngby, J. J. Mortensen, K. S. Thygesen, and K. W. Jacobsen, *Phys. Rev. Mater.* **7**, 014007 (2023).
- [37] X. Fu, T. Xie, A. S. Rosen, T. Jaakkola, and J. Smith, “MOFDiff: Coarse-grained Diffusion for Metal-Organic Framework Design,” (2023), arxiv:2310.10732 [cond-mat, physics:physics].
- [38] A. Cheng, A. Lo, S. Miret, B. Pate, and A. Aspuru-Guzik, “Reflection-Equivariant Diffusion for 3D Structure Determination from Isotopologue Rotational Spectra in Natural Abundance,” (2023), arxiv:2310.11609 [astro-ph, physics:physics].
- [39] R. Elijošius, F. Zills, I. Batatia, S. W. Norwood, D. P. Kovács, C. Holm, and G. Csányi, “Zero Shot Molecular Generation via Similarity Kernels,” (2024), arxiv:2402.08708 [physics].
- [40] Y. Song and S. Ermon, in *Advances in Neural Information Processing Systems*, Vol. 32 (Curran Associates, Inc., 2019).
- [41] N. Thomas, T. Smidt, S. Kearnes, L. Yang, L. Li, K. Kohlhoff, and P. Riley, “Tensor field networks: Rotation- and translation-equivariant neural networks for 3D point clouds,” (2018), arxiv:1802.08219 [cs].
- [42] K. Schütt, O. Unke, and M. Gastegger, in *Proceedings of the 38th International Conference on Machine Learning* (PMLR, 2021) pp. 9377–9388.
- [43] J. Gastegger, F. Becker, and S. Günnemann, in *Advances in Neural Information Processing Systems*, Vol. 34 (Curran Associates, Inc., 2021) pp. 6790–6802.
- [44] S. Batzner, A. Musaelian, L. Sun, M. Geiger, J. P. Mailoa, M. Kornbluth, N. Molinari, T. E. Smidt, and B. Kozinsky, *Nat Commun* **13**, 2453 (2022).
- [45] C. J. Pickard and R. J. Needs, *J. Phys.: Condens. Matter* **23**, 053201 (2011).
- [46] Y. Song, J. Sohl-Dickstein, D. P. Kingma, A. Kumar, S. Ermon, and B. Poole, “Score-Based Generative Modeling through Stochastic Differential Equations,” (2021), arxiv:2011.13456 [cs, stat].
- [47] H. Li, Y. Jiao, K. Davey, and S.-Z. Qiao, *Angewandte Chemie* **135**, e202216383 (2023).
- [48] P. Dhariwal and A. Nichol, “Diffusion Models Beat GANs on Image Synthesis,” (2021), arxiv:2105.05233 [cs, stat].
- [49] K. T. Schütt, H. E. Sauceda, P.-J. Kindermans, A. Tkatchenko, and K.-R. Müller, *The Journal of Chemical Physics* **148**, 241722 (2018).
- [50] K. T. Schütt, S. S. P. Hessmann, N. W. A. Gebauer, J. Lederer, and M. Gastegger, *The Journal of Chemical Physics* **158**, 144801 (2023).
- [51] P. Kostelník, N. Seriani, G. Kresse, A. Mikkelsen, E. Lundgren, V. Blum, T. Šikola, P. Varga, and M. Schmid, *Surface Science* **601**, 1574 (2007).
- [52] L. R. Merte, M. K. Bisbo, I. Sokolović, M. Setvín, B. Haggman, M. Shipilin, M. Schmid, U. Diebold, E. Lundgren, and B. Hammer, *Angewandte Chemie International Edition* **61**, e202204244 (2022).
- [53] L. R. Merte, N. Braud, L. Buß, M. K. Bisbo, H. J. Wallander, J.-O. Krisponeit, J. I. Flege, B. Hammer, J. Falta, and E. Lundgren, *J. Phys. Chem. C* **127**, 2988 (2023).
- [54] J. Derouin, R. G. Farber, M. E. Turano, E. V. Iski, and D. R. Killelea, *ACS Catal.* **6**, 4640 (2016).
- [55] B. Deng, P. Zhong, K. Jun, J. Riebesell, K. Han, C. J. Bartel, and G. Ceder, *Nat Mach Intell* **5**, 1031 (2023).
- [56] N. Rønne, M.-P. V. Christiansen, A. M. Slavensky, Z. Tang, F. Brix, M. E. Pedersen, M. K. Bisbo, and B. Hammer, *The Journal of Chemical Physics* **157**, 174115 (2022).